scientific reports

Check for updates

OPEN

Mango peels-assisted synthesis of carbon quantum dots for potential optical sensing of diazinon

Nor Afiqah Nor Asri[1], Yap Wing Fen[1,2]✉, Nurul Illya Muhamad Fauzi[2], Nur Aqilah Kamaruzzaman[1], Rahayu Emilia Mohamed Khaidir[3], Hazwani Suhaila Hashim[2], Muhammad Fahmi Anuar[2], Muhammad Amir Zakwan Mohd Zailani[2], Ahmad Danish Iskandar Mohd Fadzil[1], Nur Nadia Amira Mahamad Basari[1], Mazliana Ahmad Kamarudin[1] & Huda Abdullah[4]

Recently, carbon quantum dots (CQDs) have received widespread attention for their attractive properties and potential in sensing applications; however, their production often uses harmful materials and high energy. In this study, CQDs were acquired from mango peels using green hydrothermal method at 200 °C for 3, 6, 9, 12, and 15 h, using water as the solvent. The optical behavior of CQDs with different time synthesis, indicating photoluminescence (PL) emissions wavelength (441–447 nm), varying absorbance (0.80–0.99), and slight changes in optical bandgap (3.935–3.825 eV), showing synthesis time influences optical behavior. The CQDs with 3 h synthesis time were chosen to undergo structural characterization due to the most left shifted in PL emission, indicating the smallest particle size. Transmission electron microscopy analyzed that the CQDs were monodispersed with the average particle size was 3.54 nm, while energy dispersive X-ray results exhibited high carbon content of 97%. Fourier transform infrared analysis proves the formation of CQDs nanoparticles by the existence of hydroxyl, carbonyl, and carboxyl functional groups. Atomic force microscopy confirmed a root mean square roughness increased from 0.71 to 1.02 nm, indicating CQDs attachment, and the gold-CQDs thin film was later used as the surface plasmon resonance (SPR) sensing layer. The develop gold-CQDs thin film-based SPR sensor was successfully tested in diazinon concentration range from 0 to 100 nM, with a limit of detection as low as 0.01 nM and sensitivity of 0.0153° nM^{-1}. These results indicate that the potential of mango peels-derived CQDs as sustainable nanomaterials for optical sensing applications, particularly in environmental monitoring using SPR-based technology.

Keywords Mango peels, Carbon quantum dots, Green synthesis, Diazinon, Surface plasmon resonance

Mango (*Mangifera indica L.*) is a fruit grown worldwide, especially in Southeast Asia. It ranks 5th in fruit production with 27 million tons annually. The pulp makes up 33%–85% of the fruit and was used in various products, while the peels, around 7%–24%, was considered waste[1]. The poor management and large quantities of waste can easily lead to resource degradation and environmental problems[2]. Creating novel nanomaterials from mango peels waste for variety application is a strategic and cost-effective way to reduce those problems, and it is a successful approach of 'waste to wealth'[3, 4, 5]. Moreover, structural carbohydrates such as pectin and cellulose, which are abundant in mango peels, contribute to its high carbon content, making it potential precursors for carbon quantum dots (CQDs)[6, 7, 8, 9]. CQDs belong to the group of zero-dimensional nanostructure materials with a diameter below 10 nm in size[10, 11], known for their unique traits including tunable photoluminescence properties, low toxicity, excellent biocompatibility, high photostability, good water solubility, environmental friendly, high quantum yield, and easy surface modification[12, 13, 14, 15, 16, 17, 18].

In recent years, several studies have reported the successful derivation of CQDs from mango peels with an average particle size ranging from 3 to 8 nm, which is consistent with the standard size of CQDs which is generally

[1]Department of Physics Faculty of Science , Universiti Putra Malaysia , 43400 UPM Serdang, Selangor, Malaysia. [2]Institute of Nanoscience and Nanotechnology Functional Nanotechnology Devices Laboratory , Universiti Putra Malaysia , 43400 UPM Serdang, Selangor, Malaysia. [3]Faculty of Applied Sciences , Universiti Teknologi MARA Cawangan Sarawak , Kota Samarahan, Sarawak 94300, Malaysia. [4]Department of Electrical Electronic and System Engineering Faculty of Engineering and Built Environment , Universiti Kebangsaan Malaysia , Bangi 43600, Malaysia. ✉email: yapwingfen@upm.edu.my

below 10 nm[1, 6, 8, 9, 19, 20]. Furthermore, the production of CQDs from mango peels have been demonstrated by using various synthesis approaches, such as microwave[6], carbonization[1], and hydrothermal methods[7, 8, 19]. Among these methods, hydrothermal is the most commonly used due to its advantages such as straightforward manipulation, high yield, consistent output, low air pollution, and low energy use[20, 21, 22, 23, 24, 25, 26, 27]. The hydrothermal synthesis method produces CQDs smaller than 10 nm by heating a precursor solution in a teflon-lined autoclave under controlled temperature and pressure conditions, as reported by previous studies[28, 29, 30]. Moreover, hydrothermal synthesis aligns with green synthesis concept as it uses water as a solvent, operates under moderate temperatures, and no harmful chemicals used[26]. However, most previous papers involved prolonged reaction time to derived CQDs from mango peels. For instance, Malitha et al.[19] and Ponnusamy et al.[7] used synthesis durations of 10 and 6 h, respectively, yet provided limited insight on how synthesis time influences optical properties. Therefore, examining the effect of synthesis time is crucial to better understanding the relationship between reaction conditions and optical properties of mango peel-derived CQDs.

Over the past few years, CQDs from mango waste have been explored in various applications such as active packaging[7], photocatalytic activity[19, 31], bioimaging[6, 9, 32, 33], and optical sensing[8, 9, 34]. For optical sensing applications, detection of heavy metal ions such as Fe^{2+} [34, 9] and pesticides like mesotrione[8] have been examined by using CQDs from mango waste. Nevertheless, the application of mango peels-derived CQDs in other pesticides detection remains largely unexplored, particularly diazinon. Diazinon is an extensively utilized organophosphate pesticide applied to control pests in agriculture, but its residues can pose a harmful threat to humans, animals, and environment[35, 36, 37]. Considering the hazardous effects of diazinon, a sensitive and reliable detection method is urgently needed[38].

To address this need, surface plasmon resonance (SPR) has emerged as highly sensitive, label-free, and real time monitoring optical sensing methods[39, 40, 41, 42, 43, 44, 45, 46]. SPR refers to the simultaneous oscillation of free electrons at the interface between metal and dielectric material developed by incident light[11, 47, 48]. This phenomenon is commonly observed by using Kretschmann configuration, where the change in refractive index near the metal surface is monitored under total internal reflection conditions[48, 49]. Previous studies have incorporated various materials to enhance SPR performance for diazinon detection, including polyclonal goat anti-rabbit[50], pyrimidine[51], and thiocholine with acetylcholinesterase[52], capable to detect it down to nanomolar range[50, 52]. However, to the best of our knowledge, the integration of carbon-based materials with SPR for diazinon detection has not yet been explored, particularly CQDs. Therefore, in this research, the deposition of mango peels-derived CQDs onto a gold thin film as the sensing layer in SPR for the detection of diazinon will be fabricated for the first time. This present work evaluates the potential of SPR-based platform for the detection of diazinon using mango peels-derived CQDs as the surface modification layer. In addition, this work focuses on the green synthesis of CQDs using a short reaction time and relatively low temperature to minimize energy consumption while maintaining sustainability. The optical properties of the CQDs will be characterized by using photoluminescence (PL) and ultraviolet–visible (UV-Vis) spectroscopy, and compared across different synthesis durations, whereas structural characterization will also be conducted by using transmission electron microscopy (TEM) analysis, Fourier transform infrared (FTIR) spectra and atomic force microscopy (AFM) analysis to support and validate the experimental findings.

Materials and methods

Materials and reagents

Mango peels were collected from a nearby mango juice seller in Sri Serdang, Selangor and deionized water (DW) from the water purification system (Model: Direct Q 3UV) (Merck, Germany). PTFE lined stainless steel teflon autoclave (100 mL) was obtained from Nanjing Shuishan Technology Co., Ltd China. Nylon syringe filters with 0.22 µm were purchased from Labfil, Hangzhou City, Zhejiang, China. A stock solution of diazinon (100 µg/mL) were obtained from Sigma-Aldrich (St. Louis, MO, USA).

Preparation of chemical

DW was used to dilute stock solution of diazinon (0.33 mM) to produce a lower concentration of 0.1 mM by applying dilution formula ($M_1V_1 = M_2V_2$). Then, the 0.1 mM diazinon solution was further diluted to 0.01 mM and the step was repeated until it reached 100, 10, 1, 0.1, 0.1, and 0.01 nM.

Green-synthesis of CQDs derived from Mango peels

Green-synthesis, which is hydrothermal method, was used to derive CQDs from mango peels. The CQDs synthesis procedure was illustrated in Fig. 1. The mango peels obtained were washed thoroughly with tap water to eliminate unnecessary impurities. Then, the washed mango peels were dried in the oven (Memmert UN30, Germany) for 24 h with 80 °C to remove the moisture. The dried mango peels were ground into tinier pieces and then filtered by using sieve of 45 µm. 0.05 g of mango peels powder was weighed and mixed with 50 mL of DW in the teflon autoclave. The hydrothermal process was carried out for 3 h with a temperature of 200 °C. The reacted solution was filtered by using 0.22 µm nylon syringe filter to eliminate any precipitates, large aggregates, and unreacted residues. This fine filtration step has been reported as an effective and practical alternative to dialysis for producing optically clear CQDs dispersions[53]. These steps will be repeated for 6 h, 9 h, 12 h, and 15 h synthesis time. Subsequently, the sample was placed under ultraviolet light for visual confirmation of its photoluminescence and visually compare its appearance under daylight and ultraviolet light. The purified CQDs were kept in aqueous form for most characterizations to preserve their optical properties and active surface functional groups[54]. Meanwhile, for FTIR, AFM, and SPR analysis, the gold–CQDs thin film was prepared and air-dried at room temperature for 24 h to ensure a uniform coating and stable surface properties. The solid film was required for FTIR to analyze surface functional groups, for AFM to study surface morphology, and for SPR to evaluate the optical response of the sensor surface[55].

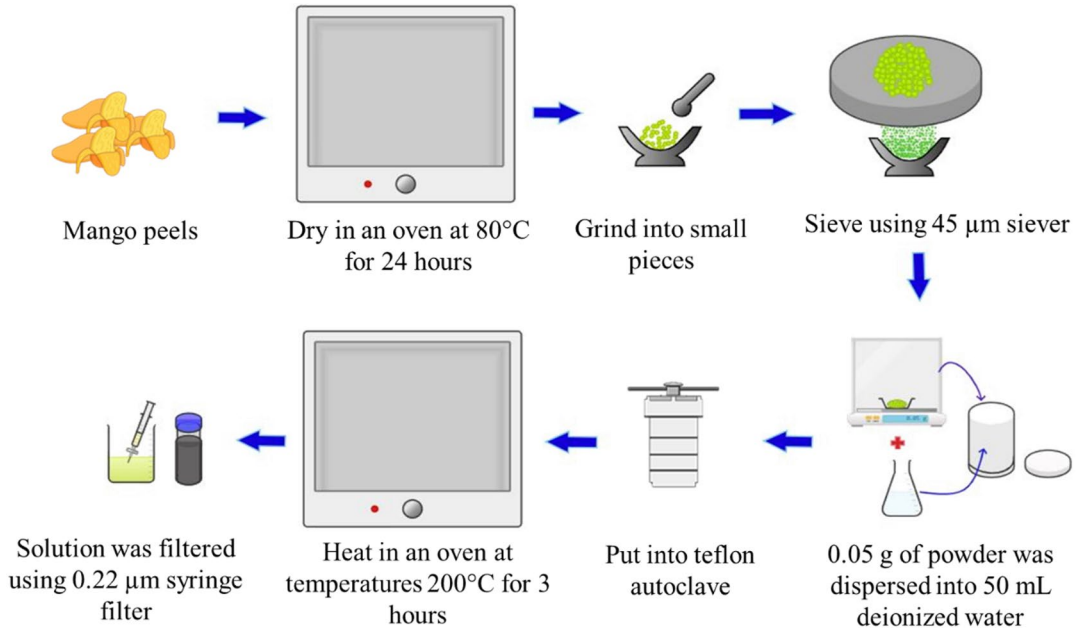

Fig. 1. A schematic diagram of hydrothermal method for the synthesis of CQDs from mango peels.

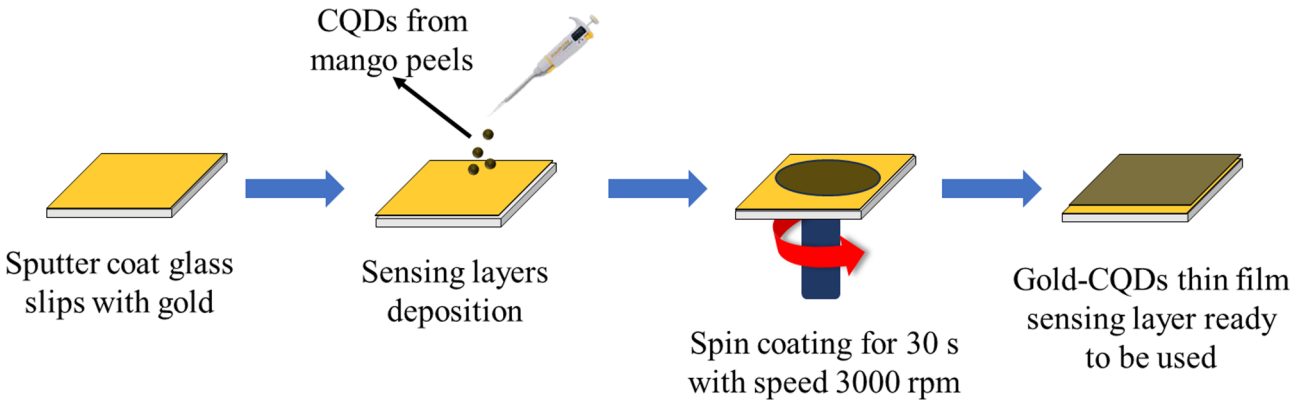

Fig. 2. Steps involved in gold-CQDs thin film preparation process.

Characterization of CQDs derived from Mango peels

Characterization of synthesized CQDs was carried out using various analytical techniques. Photoluminescence is a process where the emission of luminescence from molecules irradiated with light is detected as a function of wavelength. The photoluminescence intensity against the wavelength spectrum of CQDs were analyzed using a Perkin Elmer, LS 55 Fluorescence Spectrometer (United Kingdom) at excitation wavelengths of 365 nm. The optical absorption spectrum of the synthesized CQDs were obtained using an ultraviolet–visible spectrophotometer (UV-3600, Shimadzu, Japan). The spectrums were recorded in the wavelength range from 200 nm to 600 nm. To study shape, size, and distribution of particle size of CQDs, transmission electron microscope (TEM) (Talos L120C, United States) was used at a voltage of 120 kV. Fourier transform infrared (FTIR) spectra for CQDs were recorded in the transmittance mode using ALPHA II from Bruker, Germany. The model atomic force microscopy (AFM) employed in this work was by Bruker Crest (Billerica, Massachusetts, United States), dimension edge in ScanAsyst peak force tapping mode.

Sensing layer preparation

Firstly, the glass coverslip was cleaned with acetone to remove the dirt and fingerprints marks. Next, by using SC7640 Sputter Coater, a layer of gold thin film with a thickness approximately 50 nm was deposited on the glass substrates. Next, 1 mL of CQDs solution was placed onto the surface of gold thin film and spun at 3000 rpm for 3 s. The schematic diagram representing preparation of gold-CQDs thin film processes was shown in Fig. 2.

SPR spectroscopy

As shown in Fig. 3, SPR measurements were carried out using customized setup based on Kretschmann configuration consisting of laser, chopper, polarizer, pinhole, sensor chip, prism, rotating stage, photodiode, lock-in amplifier, stepper motor, and computer. The uncoated glass thin film was attached to one side of the prism using index-matching gel. In this study, two sensing surface configurations are provided, involving gold thin film and gold-CQDs thin film. A monochromatic He-Ne laser (632.8 nm) was used as light source, directed through the prism to excite surface plasmons by interacting with the free electron from the metal surface[41, 48]. Initially, DW was injected into a hollow sample cell to obtain reference reflectance signal using photo diode and the signal was then analyzed by the lock-in amplifier. Subsequently, diazinon solutions with different concentrations (0.01 to 100 nM) were replaced the DW that was in contact with the sensing surface.

Results and discussion

Optical properties

Comparison of CQDs under natural light and ultraviolet light

The visual appearance of the synthesized CQDs under natural and ultraviolet (UV) light was compared to provide an initial indication of their optical properties[56]. The solutions of CQDs with different synthesized time which are 3, 6, 9, 12, and 15 h were compared to each other and DW under natural light, as depicted in Fig. 4. The results indicated that CQDs synthesized with different times were pale yellow in natural light, while DW remained clear. From the results, it shows that by extending the reaction time beyond the optimal duration reduces the emitting centers, which can potentially cause fading or loss of color in solutions[57]. Meanwhile, the solution of CQDs exhibited blue fluorescent under UV-light at 365 nm, as illustrated in Fig. 5, whereas DW does not show any fluorescence towards it. The differences between various synthesized time show minimal differences, this shows

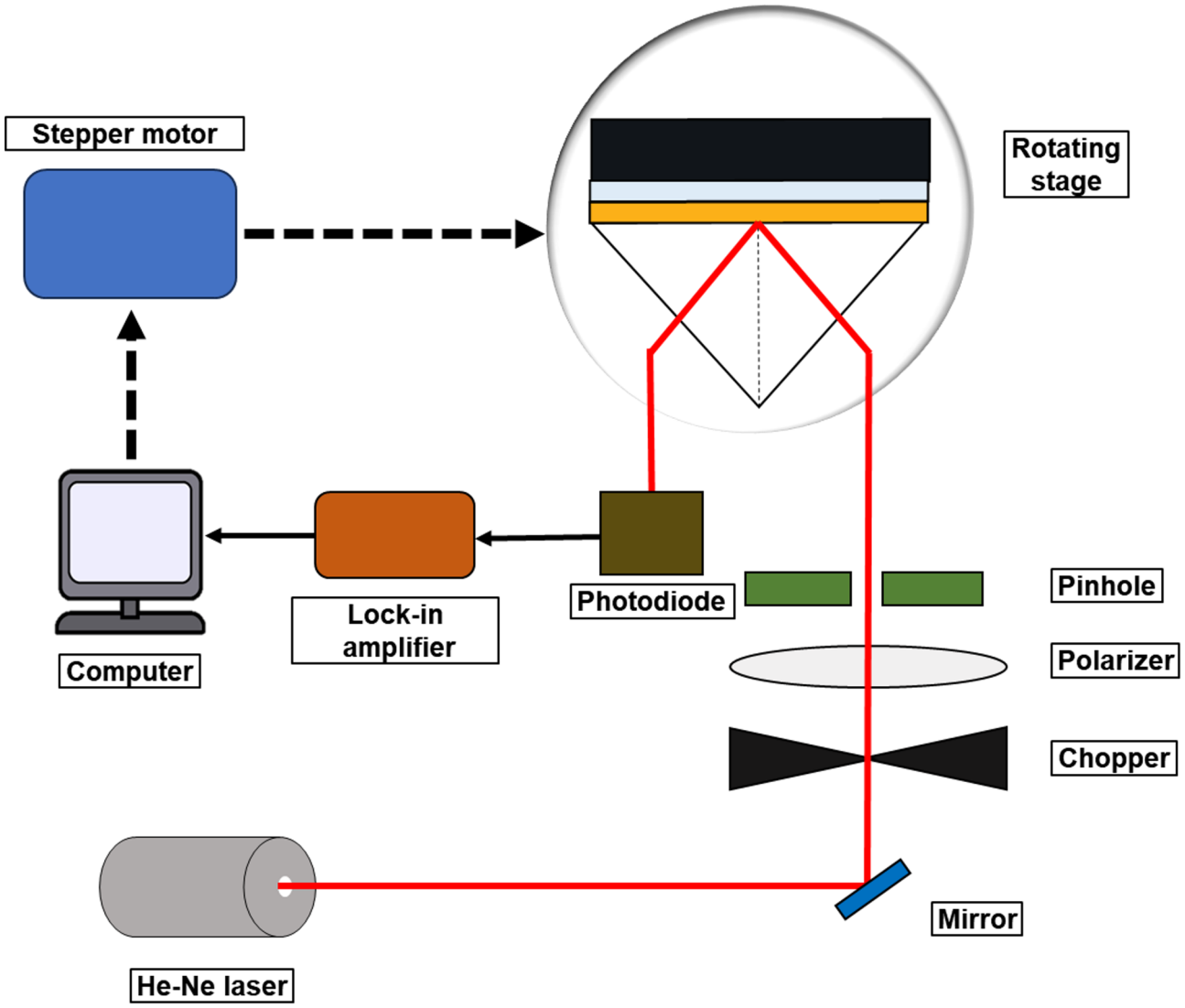

Fig. 3. Schematic diagram of surface plasmon resonance spectroscopy.

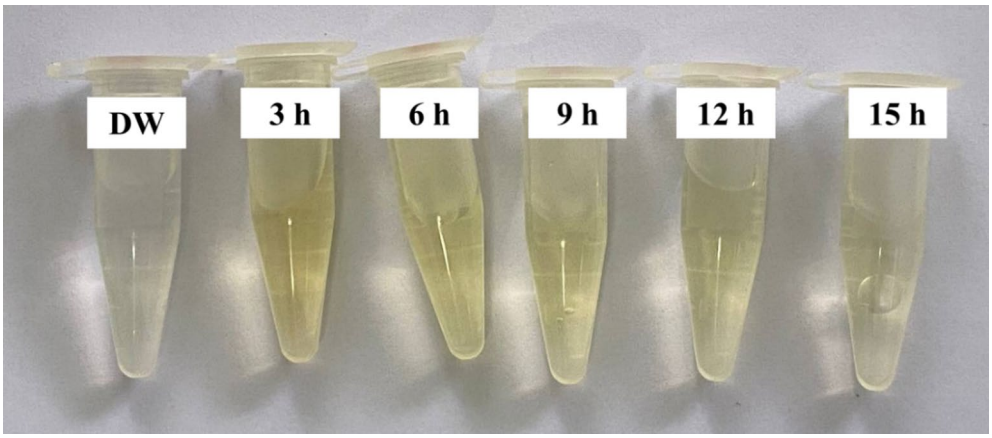

Fig. 4. CQDs derived from mango peels and DW under natural light.

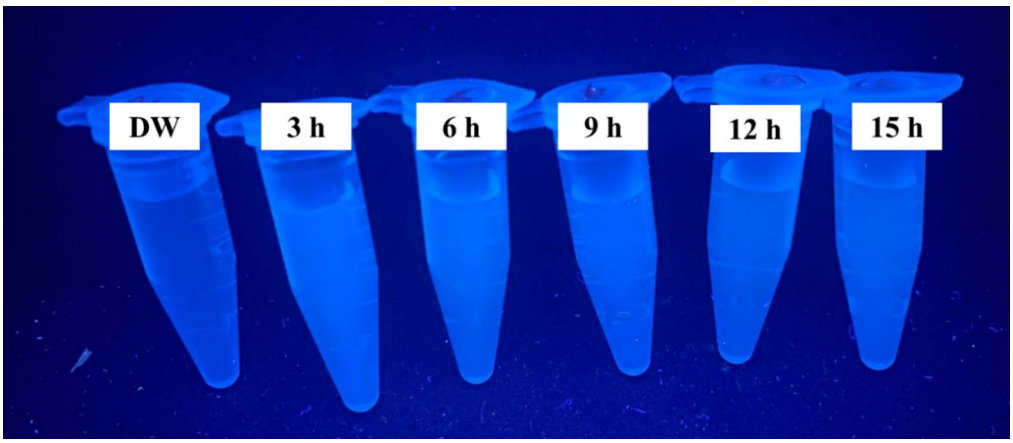

Fig. 5. CQDs derived from mango peels and DW under UV-light.

that further extending the reaction time does not significantly enhance optical properties[58]. Besides, the longer reaction time causes over-carbonization and photobleaching[59, 60, 61].

Photoluminescence spectroscopy

Photoluminescence (PL) analysis was performed to investigate the optical behavior and size-dependent emission properties of the synthesized CQDs[62, 63]. The result of PL spectroscopy of CQDs derived from mango peels synthesized over various time of heating of 3, 6, 9, 12, and 15 h were shown in Fig. 6. The PL spectrum was observed at an excitation wavelength of 365 nm, indicating a strong emission in the ultraviolet spectrum[64]. The recorded emission wavelengths were 441 nm for 3 h, 445 nm for both 6 h and 9 h, 446 nm for 12 h, and 447 nm for 15 h. The PL spectra were normalized to highlight peak shifts independent of intensity effects[65]. From the results, a consistent 4–6 nm red shift was detected, which exceeded the instrument's ± 1 nm accuracy, confirming a real optical change linked to gradual bandgap narrowing[66, 67]. Since the synthesis durations selected (3, 6, 9, 12, and 15 h) were close to each other, the structural evolution was limited, which explained the relatively small wavelength difference[68, 69]. Additionally, the minimal change in PL intensity indicates stable defect-related emission, which is typical for short incremental synthesis adjustments[69, 70]. Subsequently, the results showed that 3 h CQDs had the most left-shifted line in the PL graph, which indicated the smallest CQDs size. Based on quantum confinement effect, smaller nanoparticles indicate blue-shifted referring to shorter emission wavelengths, while larger nanoparticles tend to emit at longer emission wavelengths[71]. As the synthesis time increases, size growth rise[67].

UV-Vis spectroscopy

UV–Vis spectroscopy allowed the determination of optical absorption characteristics of nanoscale materials and provided information on the electronic transitions and surface states of CQDs[67, 72]. As shown in Fig. 6, an optical absorption of CQDs was recorded ranging from 200 to 600 nm, with absorption peaks at 281 nm (3 h), 288 nm (6 h), 286 nm (9 h), 287 nm (12 h), and 286 nm (15 h), and corresponding absorbance values of 0.80, 0.90, 0.96, 0.97, and 0.99, respectively. The CQDs exhibited peaks in the region of 281 to 288 nm, typically attributed to the

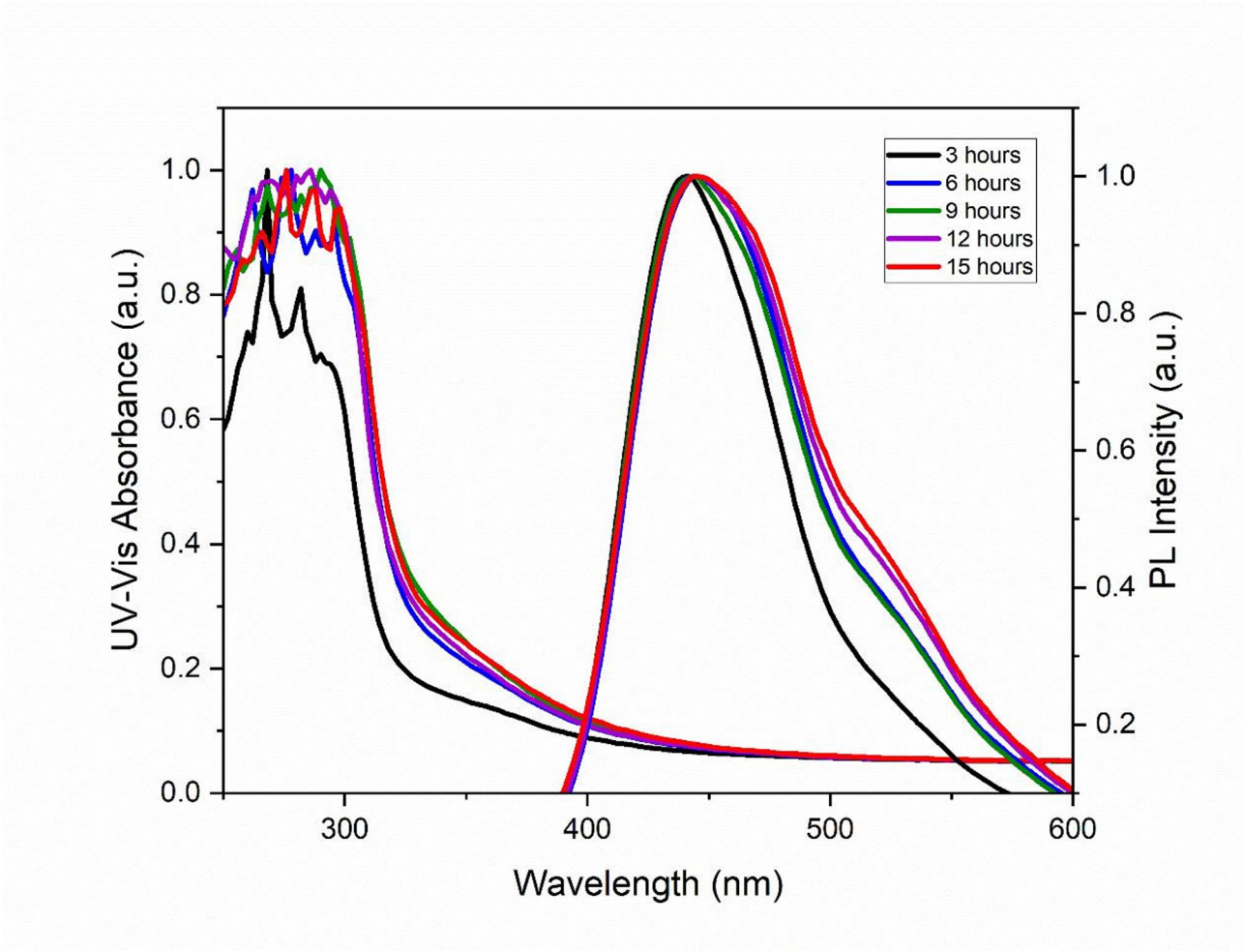

Fig. 6. UV-Vis absorbance spectrum and normalized PL spectra of CQDs synthesized from mango peels for 3, 6, 9, 12 and 15 h.

characteristic for carbon-based materials, which are π-π* transitions of aromatic sp^2 domains (C = C and C–C) and n-π* transition of C = O of graphitic core, which were important for the sensing mechanism as they reflected the active sites that could interact effectively during sensor detection[6, 19, 73]. As the synthesis time increased, the absorbance intensity rise slightly, indicating gradual carbonization[74].

Optical band gap

Optical band gap analysis was carried out to determine the energy difference between the valence and conduction bands of CQDs, thus providing insight into the optical capabilities and electronic properties of the material[75]. The minimal energy needed to move an outer-shell electron from the valence band to the conduction band was referred to optical band gap[44, 76]. The correlation between the absorption coefficient (α) and incident photon energy ($h\nu$) for the case of indirect transition of mango peels derived CQDs has a characteristic relation[77]. The Tauc plot approach was proposed to estimate the optical band gap of CQDs from different duration of heating based on the UV-Vis analysis. It is stated as:

$$(\alpha h\nu)^2 = K\,(h\nu - E_g) \tag{1}$$

Where E_g is the optical band gap and K is a constant. Figure 7 (a), (b), (c), (d) and (e) depict the relation between $(\alpha h\nu)^2$ versus $h\nu$ for CQDs that are synthesis at different times. The linear portion of the optical absorption curve was extrapolated and indicated that energy band gap value for 3 h, 6 h, 9 h, 12 h and 25 h of CQDs are 3.935 eV, 3.853 eV, 3.844 eV, 3.839 eV and 3.825 eV, respectively.

As can be shown, the calculated band gap values for CQDs synthesized at various times reveal a slight decrease from 3.935 eV (3 h) to 3.825 eV (15 h), indicating that the CQDs are getting bigger due to quantum confinement effect[67]. The optical band gap is impacted by secondary structural rearrangements resulted in prolonged synthesis times[44, 78]. Additionally, the absorbance peaks trend in UV-Vis analysis relates to the outcome of the optical band gaps[77]. High-energy transitions are visible in the absorption peak at lower wavelengths (281 nm in UV-Vis analysis), which correlates to a wider band gap (3.935 eV). The blue shift observed in both UV–Vis

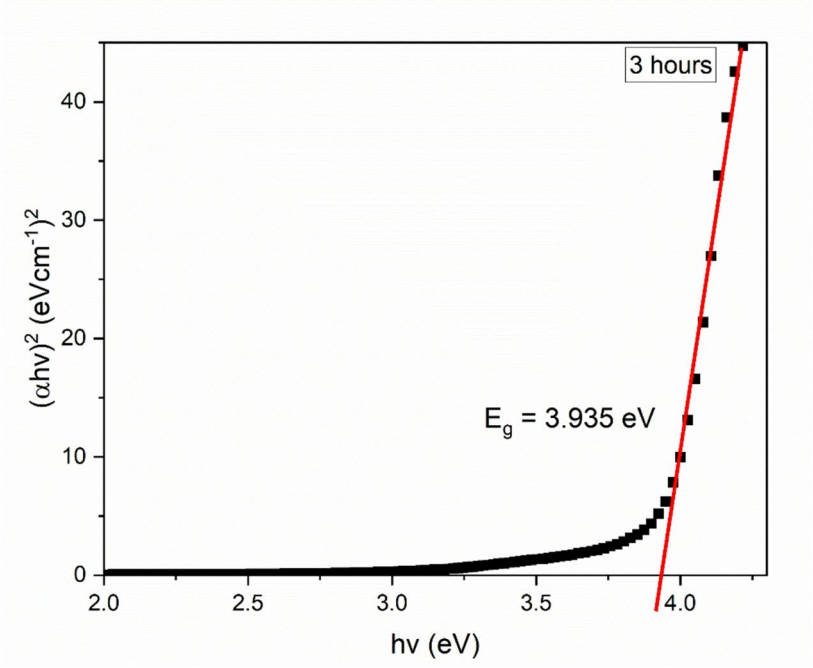

(a)

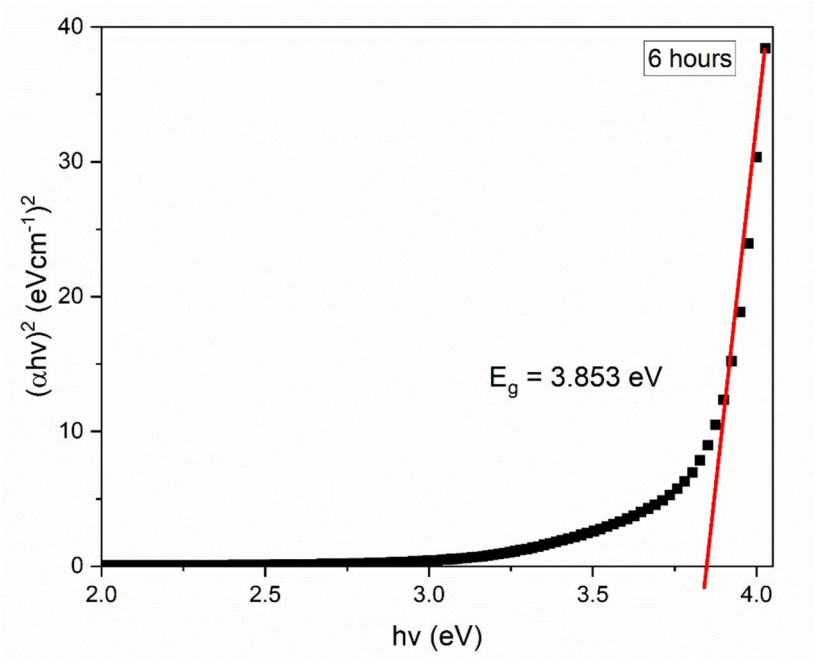

(b)

Fig. 7. Optical band gap for CQDs synthesis of (**a**) 3 h, (**b**) 6 h, (**c**) 9 h, (**d**) 12 h, and (**e**) 15 h.

absorption and PL spectra indicates the formation of smaller quantum-sized particles with increased band gap energy[67, 79, 80].

Structural and morphological properties

Transmission electron microscopy

Transmission electron microscopy (TEM) analysis was performed to observe the morphology, size, and dispersion of the synthesized CQDs, providing direct evidence of their nanoscale structure and uniformity[81].

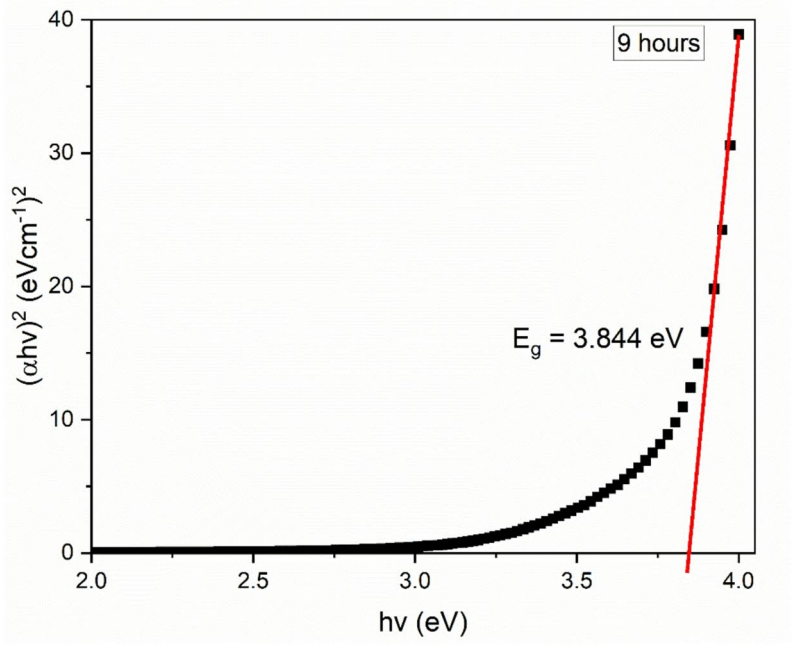

(c)

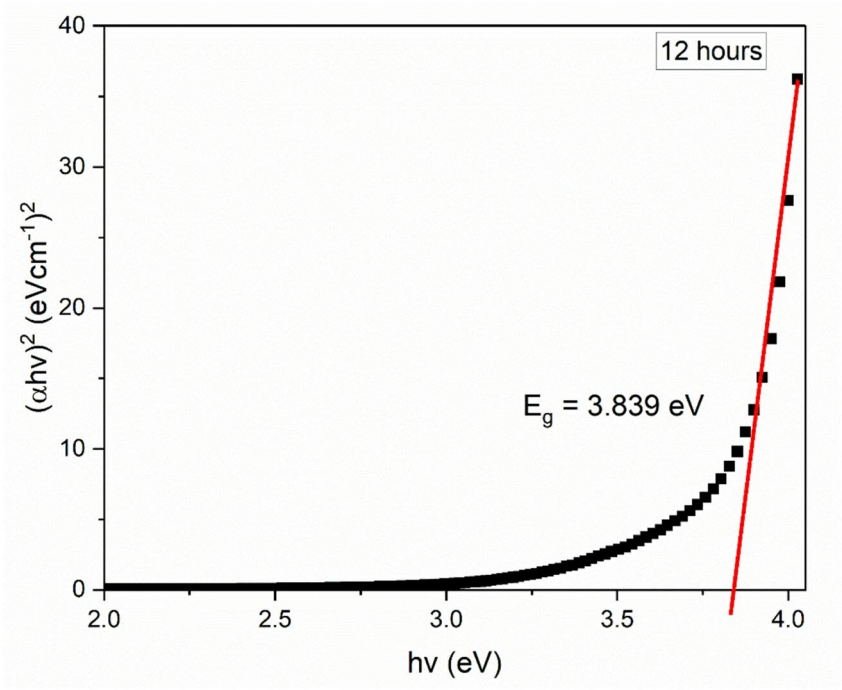

(d)

Fig. 7. (continued)

As illustrated in Fig. 8, TEM was utilized to analyze and confirm the average particle size of CQDs from mango peels that had been heated for 3 h. Moreover, the size distributions of CQDs were depicted in Fig. 9. The CQDs distribution curve revealed that the mean CQDs were 3.54 nm, and the particles were randomly dispersed, with an average particle size ranging from 1.16 to 5.53 nm. This shows that CQDs prepared from mango peels were in nano size range, validating their classification as CQDs[79, 82].

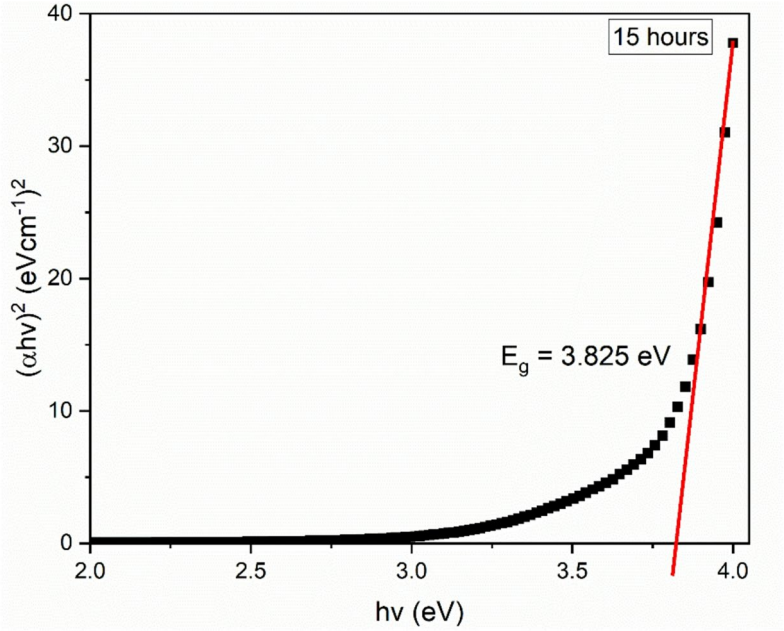

(e)

Fig. 7. (continued)

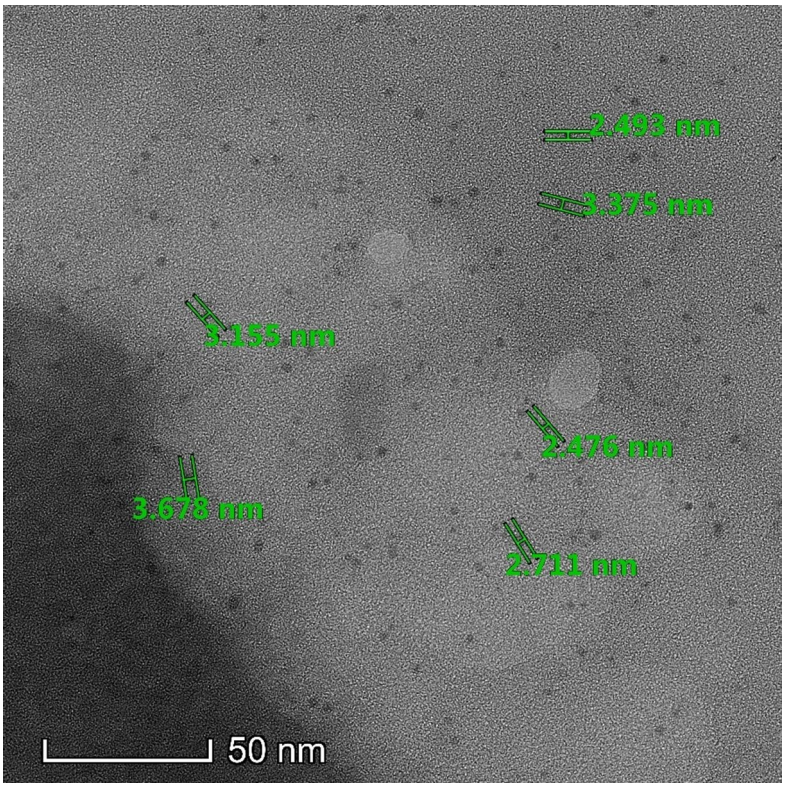

Fig. 8. TEM image of CQDs derived from mango peels at 50 nm magnification.

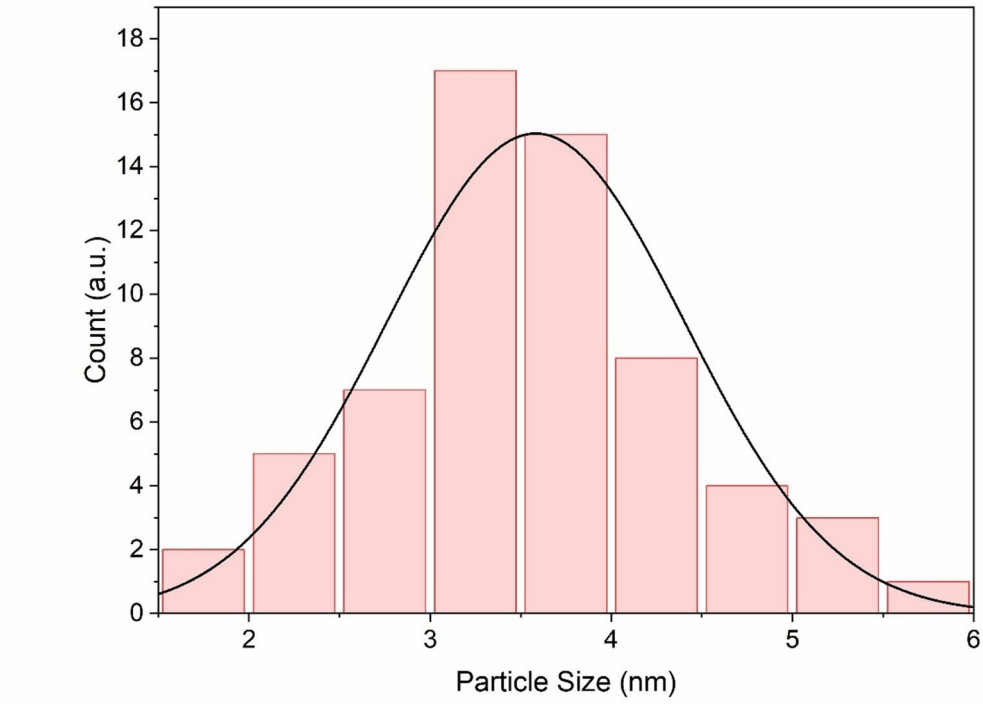

Fig. 9. Size distribution charts of CQDs derived from mango peels.

Energy dispersive X-ray

Energy dispersive X-ray microanalysis (EDX), a technique associated with electron microscopy, was carried out to determine the elemental composition of the CQDs, which works based on the production of characteristic X-rays to identify the elements present in a CQDs sample[83]. Based on Fig. 10, EDX provides an estimate of the distribution of chemical elements present in CQDs. The sample of mango peels CQDs primarily consist of carbon, which is 97%, with small amounts of oxygen and silicon which are 2.6% and 0.5% respectively. This high carbon purity of the synthesized CQDs from mango peels are primarily made up of graphitic and amorphous carbon[58]. The oxygen content of 2.6% indicates the presence of oxygen-containing functional groups, such as hydroxyl, carboxyl, and carbonyl on the surface of CQDs[19, 84, 85]. The existence of small quantity of silicon may be attributed to the natural composition of mango peels, as plant-based precursors often contain trace elements that can be incorporated into the structure of the synthesized CQDs[9, 31, 86].

Fourier transform infrared spectroscopy

Fourier transform infrared spectroscopy (FTIR) was used to analyze the functional groups on the surface of CQDs obtained from mango peels of 3 h synthesized, as shown in Fig. 11. This analysis helps to confirm the chemical bonds and elements responsible for surface passivation[87]. The broad absorption band observed around 3410 cm^{-1} corresponds to the stretching vibration of O–H groups, which can enhance electron transportability and hence supports the photocatalytic activity[88]. The peak at 2931 cm^{-1} corresponded to the C–H stretching vibration of aliphatic chains[89]. The distinct peaks appearing at 1664 cm^{-1} and 1589 cm^{-1} were attributed to the C = O and C = C stretching vibrations, respectively, suggesting the existence of carbonyl and conjugated carbon structures within the CQD framework[7, 85]. Meanwhile, the absorption peaks at 1450 cm^{-1}, 1114 cm^{-1}, and 1046 cm^{-1} correspond to C–O stretching vibrations, confirming the presence of oxygen-containing functional groups such as carboxyl or epoxy moieties[85]. Additionally, the weak peak near 666 cm^{-1} can be assigned to the C–H bending vibration[90]. These results demonstrate that the CQDs surface contains abundant hydroxyl, carbonyl, and carboxyl functional groups, which enhance their hydrophilicity and facilitate further interactions with metallic or biological surfaces, properties that are advantageous for optical sensing and surface modification applications[85, 91, 92, 93, 94].

Atomic force microscopy

The surface morphology and roughness of gold and gold-CQDs thin films were obtained using atomic force microscopy (AFM) operated in tapping mode. Figure 12 (a) and (b) reveal the two-dimensional (2D) and three-dimensional (3D) images of gold and gold-CQDs thin films, respectively. The gold thin film exhibited a uniform surface with defined grain structures[95], and the root mean square (RMS) roughness was measured to

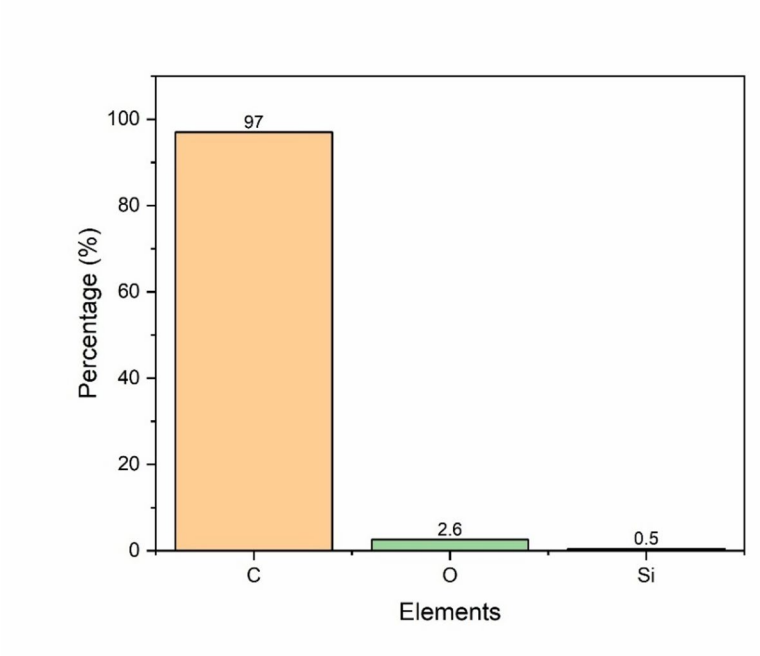

Fig. 10. EDX analysis of CQDs derived from mango peels.

be approximately 0.71 nm. In contrast, the gold-CQDs thin film displayed a more textured and granular surface due to the incorporation of spherical CQDs distributed across the gold layer, resulting in an increased RMS roughness of about 1.02 nm, indicating successful surface modification[96].

Sensing properties

SPR signal for diazinon on gold thin film

A preliminary SPR test was carried out for different concentration of diazinon ranging from 0 nM to 100 nM by using gold thin film, as depicted in Fig. 13. Firstly, DW was injected into the cell as reference solution (0 nM) and gave a resonance angle value of 53.623°. After that, the SPR experiment was continued using different concentrations of diazinon (0.01–100 nM). The resonance angle for other diazinon concentrations in contact with the bare gold thin film remained constant, as seen by the data displayed in Table 1. This may be attributed to the similar refractive index between DW and all diazinon concentrations tested, particularly at lower concentration[49]. Moreover, the bare gold thin film exhibited negligible response due to the absence of reactive sites for molecular interaction, further confirming the crucial role of CQDs in enabling effective diazinon detection through SPR mechanism[97, 98, 99].

SPR signal for diazinon on gold-CQDs thin film

The SPR measurements to detect diazinon was continued after replacing gold thin film with gold-CQDs thin film. To create the baseline for the SPR response curve, the gold-CQDs thin film was initially evaluated using DW, then were proceeded by injection of 0.01, 0.1, 1, 10, and 100 nM of diazinon aqueous solution one at a time in the hollow cell. In the case of DW in contact with gold-CQDs sensing layer, the SPR angle was 53.830° which is a bit higher than the bare gold thin film. This could be attributed to the role of CQDs as an active layer in SPR which might be able to change the refractive index of the sensing layer[47, 48]. Meanwhile, the resonance angle for diazinon concentrations of 0.01, 0.1, 1, 10, and 100 nM were 53.859°, 53.876°, 53.889°, 53.918°, and 53.924°, respectively. As illustrated in Fig. 14, the SPR curves have been shifted to the right when the concentration of diazinon increased. This indicates that the resonance angle increases with increasing diazinon concentration, most likely as a result of an increase in the refractive index of the solution[49, 100]. Additionally, this shift might have occurred as diazinon molecules interacted with the hydroxyl (–OH) and carbonyl (C = O) groups on the CQDs surface through hydrogen bonding and dipole-dipole interactions[101, 102]. The PL, UV–Vis, and FTIR results confirmed these surface functional groups and π–π* transitions, while TEM analysis showed CQDs smaller than 10 nm, providing a high surface area that enhanced adsorption, as stated in characterization section. Moreover, the polar P = O and C–N bonds in diazinon further facilitated hydrogen bonding and π–π stacking with CQDs[53, 101, 103], leading to a measurable resonance angle shift. Besides, the lowest concentration of target solution that can be obtained from the baseline signal sensor known as the limit of detection (LOD)[49, 104]. Therefore, the LOD for detection diazinon based-SPR sensor by using gold-CQDs thin film is 0.01 nM.

To analyze the sensing parameters of the SPR sensor, it is necessary to measure the resonance angle shifts at varying concentrations of diazinon. Based on data from Table 2, the shift of the resonance angle was calculated by subtracting the resonance angle of different concentration of diazinon with the resonance angle of DW. The sensitivity of this sensor can be determined by plotting the resonance angle shift against the concentration

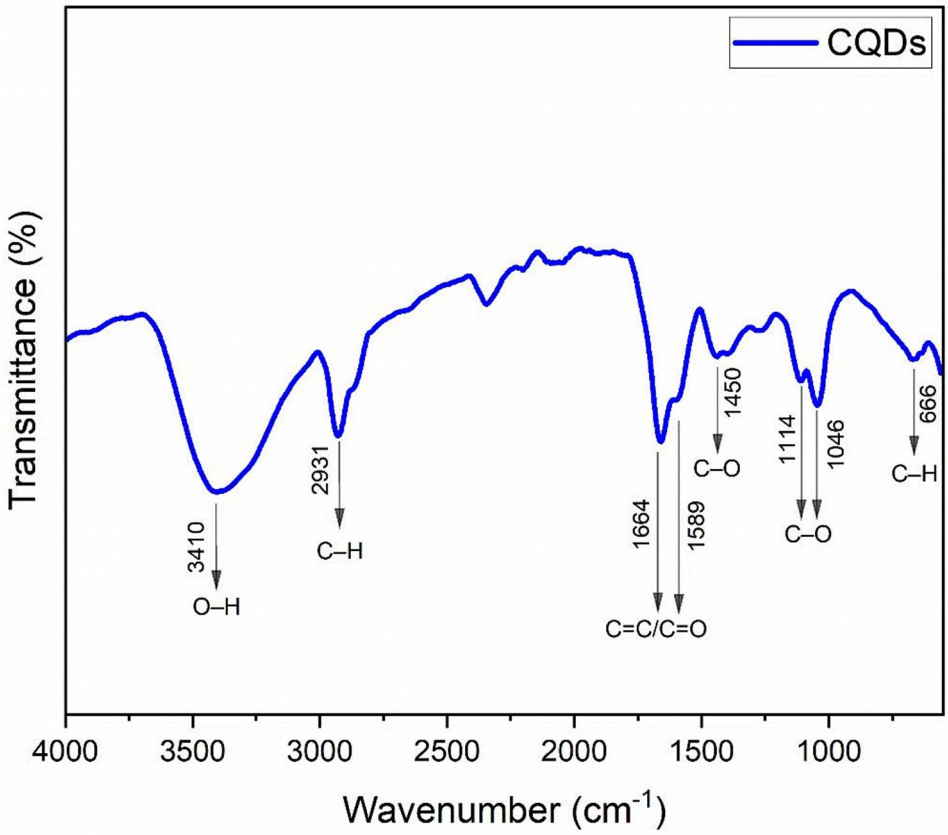

Fig. 11. FTIR pattern of 3 h synthesized CQDs from mango peels.

of diazinon as shown in Fig. 15. To further evaluate the reproducibility, the SPR sensing measurements were repeated five times under identical experimental conditions. The resulting data, presented with error bars representing the standard error of the mean, showed small deviations, indicating consistent performance[105]. From the linear regression analysis, a slope of 0.0153 was obtained with a correlation coefficient of $R^2 = 0.99597$, for the diazinon concentration range from 0.01 nM to 100 nM. Ultimately, the gold-CQDs thin film based SPR sensor demonstrated the ability to detect diazinon at a minimum concentration of 0.01 nM, with a sensitivity of 0.0153^{o} nM^{-1}.

Furthermore, to better understand the performance of the developed sensor, a comparison with previously reported SPR and plasmonic sensors for diazinon detection was conducted, as summarized in Table 3. In earlier studies, metallic nanoparticles, enzymes, and antibodies were commonly employed as recognition or sensing elements to achieve sensitivity. However, these materials often require complex preparation procedures, involve higher costs, and exhibit limited long-term stability[97,106]. In contrast, the gold–CQDs thin film synthesized from mango peels through a green synthesis method in this work achieved a low limit of detection (0.01 nM) with a suitable linear range (0–100 nM). This finding suggests that the integration of gold nanoparticles with CQDs derived from natural precursors can enhance the optical response while providing a stable, reproducible, and environmentally friendly sensing platform for diazinon detection.

Conclusion

In summary, simple, cost-effective, and green synthesis of CQDs derived from mango peels have been designed in this study. These findings show that CQDs synthesized at 3 h exhibited the most optimal optical properties, showing strong and stable photoluminescence emission at 441 nm, a distinct π–π^* transition peak in the UV–Vis spectrum around 281 nm, and the highest optical band gap value of 3.935 eV, confirming that a short synthesis time was sufficient to produce high-quality CQDs, and was therefore selected for further structural characterization. TEM displayed that the average size of CQDs derived from mango peels was 3.54 nm, confirmed the size of CQDs which is less than 10 nm. Besides, EDX analysis indicated a high carbon content of 97% with minimal impurities. The occurrence of C = O, C = C, C–H, C–O, and O–H functional groups further verified the successful formation of CQDs. The increase in RMS roughness from 0.71 nm to 1.02 nm confirmed

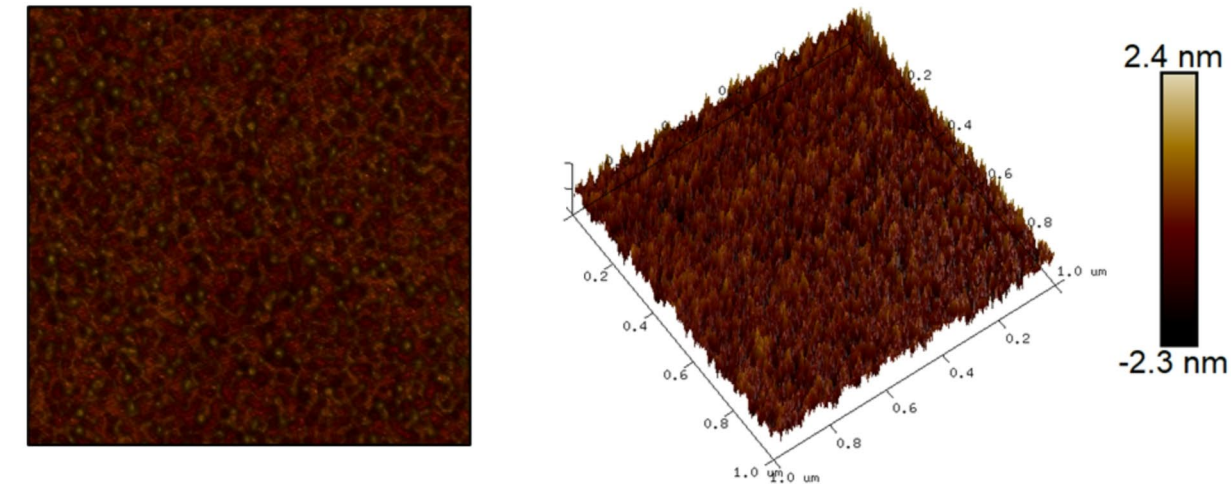

(a)

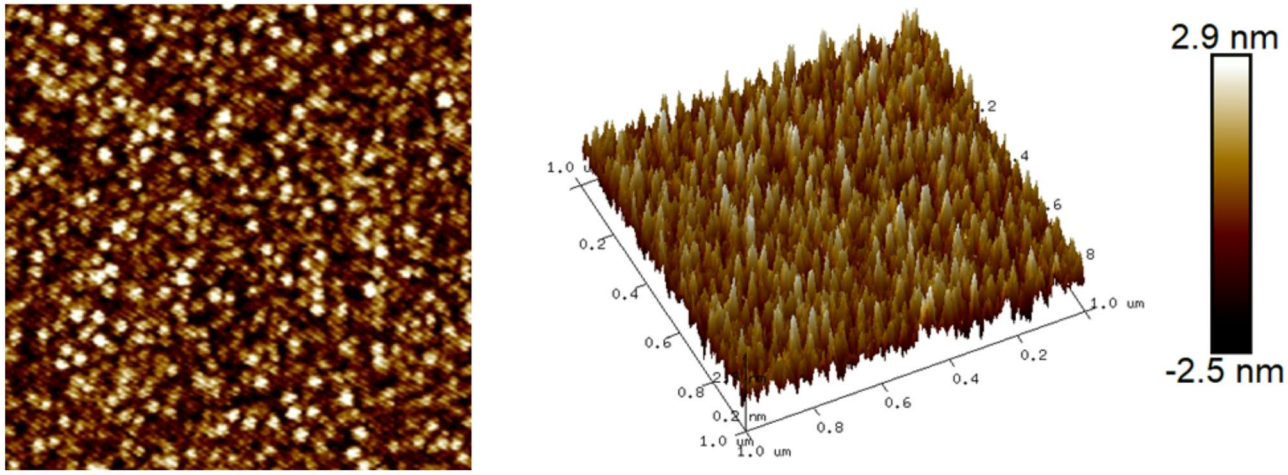

(b)

Fig. 12. AFM analysis of (**a**) gold thin film and (**b**) gold-CQDs thin film.

that CQDs were successfully deposited on the gold thin film surface. Eventually, the prepared gold-CQDs thin film served as sensing layer in a SPR system, CQDs significantly improved sensor performance, enabling the detection of diazinon solutions at very low concentrations. The developed sensor recorded a LOD as low as 0.01 nM, and a sensitivity as high as 0.0153^{o} nM^{-1}, thus proving the effectiveness of CQDs as sensing layer materials in SPR application. Hence, the results of this study highlight the potential use of gold-CQDs thin film to enhance the sensitivity of the SPR sensor for diazinon detection.

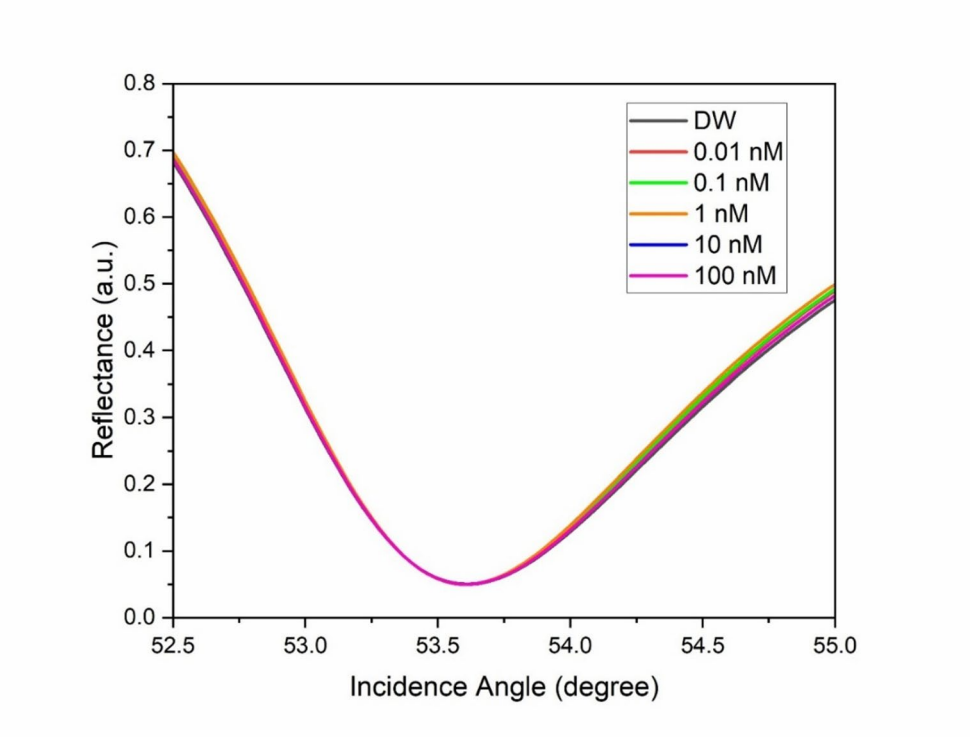

Fig. 13. The curves of SPR reflectivity of gold thin film exposed to diazinon solution of concentrations between 0 to 100 nM.

Diazinon concentration(nM)	Resonance angle (°)	Shift of resonance angle, Δθ (°)
0	53.623	0
0.01	53.623	0
0.1	53.623	0
1	53.623	0
10	53.623	0
100	53.623	0

Table 1. Resonance angle and resonance angle shift of gold thin film for detection of diazinon (0.01 nM – 100 nM).

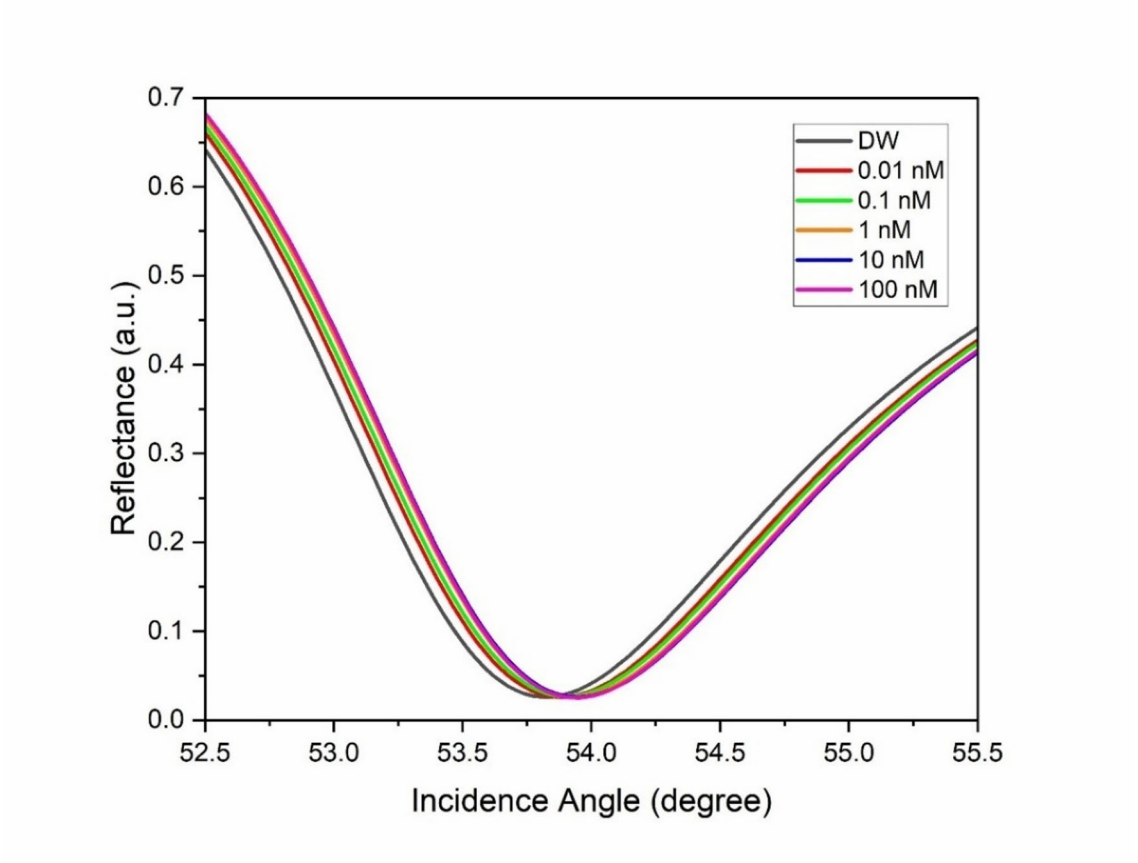

Fig. 14. The curves of SPR reflectivity of gold-CQDs thin film exposed to diazinon solution of concentrations between 0 to 100 nM.

Diazinon concentration(nM)	Resonance angle (°)	Shift of resonance angle, Δθ (°)
0	53.830	0
0.01	53.859	0.029
0.1	53.876	0.046
1	53.889	0.059
10	53.918	0.088
100	53.924	0.094

Table 2. Resonance angle and resonance angle shift of gold-CQDs thin film for detection of diazinon (0.01 nM – 100 nM).

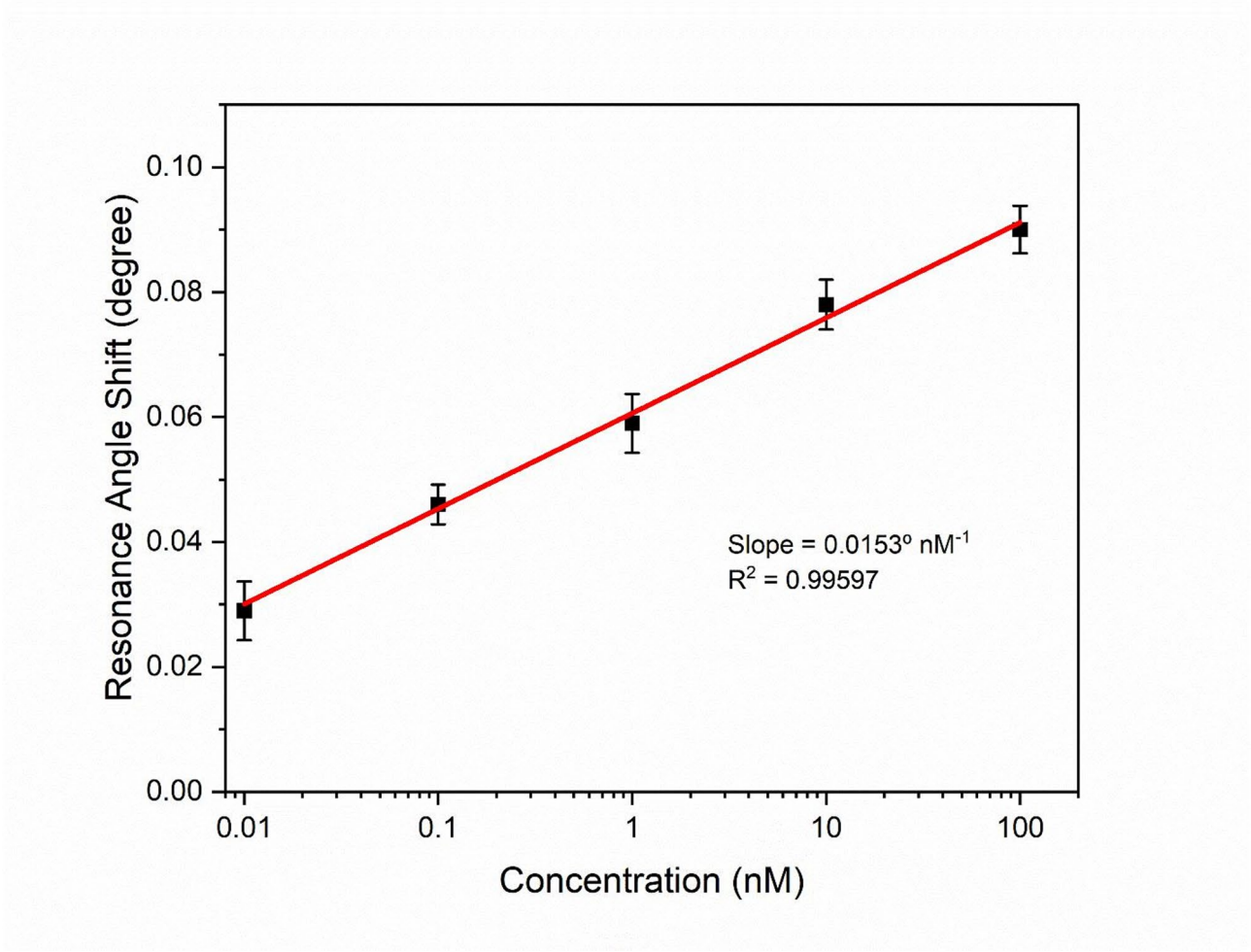

Fig. 15. Resonance angle shift of gold-CQDs thin film for sensing diazinon (0–100 nM).

Materials	Limit of Detection (LOD)	Linear Range	References
Polyclonal goat anti-rabbit (IgG)	3.29 nM	0.328–32.8 µM	50
Citrate-capped Silver Nanoparticles	0.12 µM	2–80 µM	107
Silver Nanoparticles with pyrimidine N, S moieties	23.0 nM	65.7 nM–1.97 µM	51
Thiocholine (TCh) & Acetylcholinesterase (AChE)	0.66 nM	1.0–56.8 nM	52
Gold-Candida Rugosa (microbial source) (CRL)	0.01 µM	0.01–50 µM	108
Gold- Porcine Pancreas (animal source) (PPL)	0.1 µM	0.1–50 µM	108
Gold nanoparticles (AuNPs), Hexagonal Boron Nitride (h-BN)	6.8 pM	0.01–10,000 nM	109
Gold-CQDs thin film (Mango peels-derived CQDs)	**0.01 nM**	**0–100 nM**	***This work***

Table 3. Comparison of diazinon detection performance of SPR and plasmonic-based sensors.

Data availability

All data generated or analyzed during this study are included in this published article.

Received: 15 August 2025; Accepted: 17 December 2025
Published online: 31 January 2026

References

1. Kukreja, D., Mathew, J., Lakshmipathy, R. & Sarada, N. C. Synthesis of fluorescent carbon dots from mango peels. *Int. J. ChemTech Res.* **8**, 61–64 (2015).
2. Baweja, H. & Jeet, K. Economical and green synthesis of graphene and carbon quantum dots from agricultural waste. *Mater. Res. Express*. **6**, 0850g8 (2019).

3. Kasinathan, K., Samayanan, S., Marimuthu, K. & Yim, J. H. Green synthesis of multicolour fluorescence carbon quantum dots from sugarcane waste: investigation of mercury (II) ion sensing, and bio-imaging applications. *Appl. Surf. Sci.* **601**, 154266 (2022).
4. Boruah, A., Saikia, M., Das, T., Goswamee, R. L. & Saikia, B. K. Blue-emitting fluorescent carbon quantum dots from waste biomass sources and their application in fluoride ion detection in water. *J. Photochem. Photobiol B Biol.* **209**, 111940 (2020).
5. Tyagi, A., Tripathi, K. M., Singh, N., Choudhary, S. & Gupta, R. K. Green synthesis of carbon quantum dots from lemon peel waste: applications in sensing and photocatalysis. *RSC Adv.* **6**, 72423–72432 (2016).
6. Hua, J., Hua, P. & Qin, K. Tunable fluorescent biomass-derived carbon dots for efficient antibacterial action and bioimaging. *Colloids Surf. Physicochem Eng. Asp*. **680**, 132672 (2024).
7. Ponnusamy, A. et al. Active packaging film based on chitosan/gelatin blend incorporated with mango peel carbon dots: properties and shelf life extension of minced pork. *Int. J. Biol. Macromol.* **288**, 138692 (2025).
8. Sun, X., Liu, Y., Niu, N. & Chen, L. Synthesis of molecularly imprinted fluorescent probe based on biomass-derived carbon quantum dots for detection of mesotrione. *Anal. Bioanal Chem.* **411**, 5519–5530 (2019).
9. Jiao, X. Y. et al. The synthesis of fluorescent carbon dots from mango peel and their multiple applications. *Colloids Surf. Physicochem Eng. Asp.* **577**, 306–314 (2019).
10. Zhu, J. et al. Waste utilization of synthetic carbon quantum dots based on tea and peanut shell. *J. Nanomater.* **7965756** (2019).
11. Rana, A., Yadav, K. & Jagadevan, S. A comprehensive review on green synthesis of nature-inspired metal nanoparticles: mechanism, application and toxicity. *J. Clean. Prod.* **272**, 122880 (2020).
12. García-Salcedo, Á. J., Giraldo-Pinto, L. Á., Márquez-Castro, D. J. & Tirado-Mejía, L. Influence of synthesis parameters on the optical properties of carbon dots. *Carbon Trends*. **17**, 100403 (2024).
13. Korkut, S., Vatanpour, V. & Koyuncu, I. Carbon-based quantum dots in fabrication and modification of membranes: a review. *Sep. Purif. Technol.* **326**, 124876 (2023).
14. Cui, L., Ren, X., Wang, J. & Sun, M. Synthesis of homogeneous carbon quantum dots by ultrafast dual-beam pulsed laser ablation for bioimaging. *Mater. Today Nano.* **12**, 100091 (2020).
15. Mmelesi, O. K., Mguni, L. L., Li, F., tang, Nkosi, B. & Liu, X. Recent development in fluorescent carbon quantum dots-based photocatalysts for water and energy applications. *Mater. Sci. Semicond. Process.* **181**, 108661 (2024).
16. Liu, M., Xu, Y., Niu, F., Gooding, J. J. & Liu, J. Carbon quantum dots directly generated from electrochemical oxidation of graphite electrodes in alkaline alcohols and the applications for specific ferric ion detection and cell imaging. *Analyst* **141**, 2657–2664 (2016).
17. Limosani, F. et al. Top-down n-doped carbon quantum dots for multiple purposes: heavy metal detection and intracellular fluorescence. *Nanomaterials* **11** (9), 2249 (2021).
18. Chen, Z. et al. A review of top-down strategies for the production of quantum-sized materials. *Small Sci.* **3**, 2300086 (2023).
19. Malitha, M. D., Molla, M. T. H., Bashar, M. A., Chandra, D. & Ahsan, M. S. Fabrication of a reusable carbon quantum dots (CQDs) modified nanocomposite with enhanced visible light photocatalytic activity. *Sci. Rep.* **14**, 1–18 (2024).
20. Nugraha, M. W., Zainal Abidin, N. H. & Sambudi, N. S. Synthesis of tungsten oxide/ amino-functionalized sugarcane bagasse derived-carbon quantum dots (WO3/N-CQDs) composites for methylene blue removal. *Chemosphere* **277**, 130300 (2021).
21. Singh, H., Bamrah, A., Khatri, M. & Bhardwaj, N. One-pot hydrothermal synthesis and characterization of carbon quantum dots (CQDs). *Mater. Today Proc.* **28**, 1891–1894 (2020).
22. Qurtulen et al. Elucidating the photocatalytic mechanism of biomass-derived carbon dots nanocomposite for efficient degradation of MB and CR dyes: insights into protein binding applications. *Diam. Relat. Mater.* **149**, 111547 (2024).
23. Rosales, S. et al. Simultaneous detection of carbon quantum dots as tracers for interwell connectivity evaluation in a pattern with two injection wells. *Nanomaterials* **14**, (2024).
24. Omran, B. A., Whitehead, K. A. & Baek, K. Colloids and surfaces B: biointerfaces one-pot bioinspired synthesis of fluorescent metal chalcogenide and carbon quantum dots : applications and potential biotoxicity. *Colloids Surf. B Biointerfaces*. **200**, 111578 (2021).
25. Kong, J. et al. Carbon quantum dots: properties, preparation, and applications. *Molecules* **29**, 2002 (2024).
26. Omar, N. A. S. et al. A review on carbon dots: synthesis, characterization and its application in optical sensor for environmental monitoring. *Nanomaterials* **12**, 2365 (2022).
27. Banihashem, S. M., Moradi, A., Evazzadeh, B., Namvar, F. & Fang, Z. N. Biogenically synthesized nanoparticles in wastewater treatment; a greener approach: a review. *Clean. Technol. Environ. Policy.* **26**, 1731–1754 (2024).
28. Ghosh, B. & Shirahata, N. Colloidal silicon quantum dots: synthesis and luminescence tuning from the near-UV to the near-IR range. *Sci. Technol. Adv. Mater.* **15**, 014207 (2014).
29. Ganguly, S., Das, P., Banerjee, S. & Das, N. C. Advancement in science and technology of carbon dot-polymer hybrid composites: A review. *Funct Compos. Struct* **1**, 022001 (2019).
30. Manikandan, V. & Lee, N. Y. Green synthesis of carbon quantum dots and their environmental applications. *Environ. Res.* **212**, 113283 (2022).
31. Saini, S. et al. Sustainable synthesis of biomass-derived carbon quantum dots and their catalytic application for the assessment of α,β-unsaturated compounds. *RSC Adv.* **12**, 32619–32629 (2022).
32. Jain, S., Sahu, N., Bhatia, D. & Yadav, P. Cellular uptake and viability switching in the properties of lipid coated carbon quantum dots for potential bioimaging and therapeutics. *Nanoscale Adv.* **6**, 5069–5079 (2024).
33. Pramanik, A. et al. Designing highly crystalline multifunctional multicolor-luminescence nanosystem for tracking breast cancer heterogeneity. *Nanoscale Adv.* **1**, 1021–1034 (2019).
34. Singh, J. et al. Highly fluorescent carbon dots derived from mangifera indica leaves for selective detection of metal ions. *Sci. Total Environ.* **720**, 137604 (2020).
35. Tafreshi, F. A., Fatahi, Z., Ghasemi, S. F., Taherian, A. & Esfandiari, N. Ultrasensitive fluorescent detection of pesticides in real sample by using green carbon dots. *PLoS One*. **15**, 1–17 (2020).
36. Shekarbeygi, Z., Farhadian, N., Khani, S., Moradi, S. & Shahlaei, M. The effects of rose pigments extracted by different methods on the optical properties of carbon quantum dots and its efficacy in the determination of diazinon. *Microchem J.* **158**, 105232 (2020).
37. Zahirifar, F., Rahimnejad, M., Abdulkareem, R. A. & Najafpour, G. Determination of diazinon in fruit samples using electrochemical sensor based on carbon nanotubes modified carbon paste electrode. *Biocatal. Agric. Biotechnol.* **20**, 101245 (2019).
38. Phuc, H. et al. Enhancement of carbon quantum dot luminescence efficiency through N, S co – doping for rapid ion Fe^{3+} detection. *Opt. Quantum Electron.* **57**, 1–20 (2025).
39. Anas, N. A. A. et al. Optical properties of chitosan/hydroxyl-functionalized graphene quantum dots thin film for potential optical detection of ferric (III) ion. *Opt. Laser Technol.* **120**, 105724 (2019).
40. Omar, N. A. S. et al. Quantitative and selective surface plasmon resonance response based on a reduced graphene oxide–polyamidoamine nanocomposite for detection of dengue virus E-proteins. *Nanomaterials* **10**, 569 (2020).
41. Eddin, F. B. K., Fen, Y. W., Omar, N. A. S., Liew, J. Y. C. & Daniyal, W. M. E. M. M. Femtomolar detection of dopamine using surface plasmon resonance sensor based on chitosan/graphene quantum dots thin film. *Spectrochim Acta - Part. Mol. Biomol. Spectrosc.* **263**, 120202 (2021).
42. Park, J. H., Cho, Y. W. & Kim, T. H. Recent advances in surface plasmon resonance sensors for sensitive optical detection of pathogens. *Biosensors* **12**, 180 (2022).

43. Yin, C. et al. Turn-on fluorescent inner filter effect-based B,S,N co-doped carbon quantum dots and vanadium oxide nanoribbons for α-glucosidase activity detection. *Microchem J.* **178**, 107405 (2022).
44. Tang, Y., Zeng, X. & Liang, J. Surface plasmon resonance: an introduction to a surface spectroscopy technique. *J. Chem. Educ.* **87**, 742–746 (2010).
45. Kumar, N. & Khangwal, I. Functional attributes and bio-prospects of fruit peel waste. *Foods Raw Mater.* **14**, 84–103 (2026).
46. Saleviter, S. et al. Design and analysis of surface plasmon resonance optical sensor for determining cobalt ion based on chitosan-graphene oxide decorated quantum dots-modified gold active layer. *Opt. Express*. **27**, 32294 (2019).
47. Daniyal, W. M. E. M. M. et al. Enhancing the sensitivity of a surface plasmon resonance-based optical sensor for zinc ion detection by the modification of a gold thin film. *RSC Adv.* **9**, 41729–41736 (2019).
48. Daniyal, W. M. E. M. M., Fen, Y. W., Abdullah, J., Sadrolhosseini, A. R. & Mahdi, M. A. Design and optimization of surface plasmon resonance spectroscopy for optical constant characterization and potential sensing application: theoretical and experimental approaches. *Photonics* **8**, 361 (2021).
49. Hashim, H. S. et al. Surface plasmon resonance sensor based on gold-graphene quantum dots thin film as a sensing nanomatrix for phenol detection. *Opt. Laser Technol.* **168**, 109816 (2024).
50. Yang, G. & Kang, S. Detection of multi-class pesticide residues using surface plasmon resonance based on polyclonal antibody. *Food Sci. Biotechnol.* **17** (3), 547–552 (2008).
51. Shrivas, K. et al. Silver nanoparticles for selective detection of phosphorus pesticide containing π-conjugated pyrimidine nitrogen and sulfur moieties through non-covalent interactions. *J. Mol. Liq.* **275**, 297–303 (2019).
52. Satnami, M. L. et al. Gold nanoprobe for inhibition and reactivation of acetylcholinesterase: an application to detection of organophosphorus pesticides. *Sens. Actuators B Chem.* **267**, 155–164 (2018).
53. Sousa, H. B. A., Martins, C. S. M. & Prior, J. A. V. You don't learn that in school: an updated practical guide to carbon quantum dots. *Nanomaterials* **11**, 1–88 (2021).
54. Afifah, N. et al. Localized surface plasmon resonance decorated with carbon quantum dots and triangular ag nanoparticles for chlorophyll detection. *Nanomaterials* **12**, 35 (2022).
55. Eddin, F. B. K. et al. Simultaneous measurement of the refractive index and thickness of graphene oxide/gold multilayered structure for potential in dopamine sensing using surface plasmon resonance spectroscopy. *Optik (Stuttg).* **278**, 170703 (2023).
56. Dhariwal, J., Rao, G. K. & Vaya, D. Recent advancements towards the green synthesis of carbon quantum dots as an innovative and eco-friendly solution for metal ion sensing and monitoring. *RSC Sustain.* **2**, 11–36 (2023).
57. Tong, Y. J. et al. High-quality full-color carbon quantum dots synthesized under an unprecedentedly mild condition. *iScience* **25**, 6 (2022).
58. Thakur, S. et al. Synthesis of hydrothermal-assisted papaya peel-derived carbon quantum dots impregnated carboxymethyl cellulose and pectin crosslinked nanohydrogel for shelf-life enhancement of strawberry. *Int. J. Biol. Macromol.* **283**, 137591 (2024).
59. Abd Elhaleem, S. M., Belal, F., El-Shabrawy, Y. & El-Maghrabey, M. Self-ratiometric fluorescence approach based on room-temperature instantaneously synthesized carbon dots from folin's reagent and ethanolamine for determination of nitroxinil in water, milk, and food samples. *Anal. Chim. Acta*. **1323**, 343061 (2024).
60. Ishak, N., Galář, P., Mekkat, R., Grandcolas, M. & Šoóš, M. Fine-tuning photoluminescence and photocatalysis: exploring the effects of carbon quantum dots synthesis and purification on g-C3N4. *Colloids Surf. Physicochem Eng. Asp*. **706**, 135789 (2025).
61. Wang, W., Damm, C., Walter, J., Nacken, T. J. & Peukert, W. Photobleaching and stabilization of carbon nanodots produced by solvothermal synthesis. *Phys. Chem. Chem. Phys.* **18**, 466–475 (2016).
62. Thyda, L. et al. Green synthesis of carbon quantum dots derived from mango-leaves (M – CQDs): M – CQDs/ZnO nanorods heterostructure thin films for efficient self-powered UV photodetector applications. *Appl. Surf. Sci.* **685**, 162032 (2025).
63. Dua, S. et al. Stability of carbon quantum dots: a critical review. *RSC Adv.* **13**, 13845–13861 (2023).
64. Chen, K., Zhang, M., Bhandari, B. & Deng, D. 3D printed cinnamon essential oil/banana peel carbon dots loaded corn starch/gelatin bilayer film with enhanced functionality for food packaging application. *Food Chem.* **448**, 139176 (2024).
65. Guo, H. et al. Machine learning-guided realization of full-color high-quantum-yield carbon quantum dots. *Nat. Commun.* **15**, 1–10 (2024).
66. Mohanaraman, S. P. & Chidambaram, R. A holistic review on red fluorescent graphene quantum dots, its synthesis, unique properties with emphasis on biomedical applications. *Heliyon* **10**, e35760 (2024).
67. Watcharamongkol, T., Khaopueak, P., Seesuea, C. & Wechakorn, K. Green hydrothermal synthesis of multifunctional carbon dots from cassava pulps for metal sensing, antioxidant, and mercury detoxification in plants. *Carbon Resour. Convers.* **7**, 100206 (2024).
68. Wang, S., Chen, Z. G., Cole, I. & Li, Q. Structural evolution of graphene quantum dots during thermal decomposition of citric acid and the corresponding photoluminescence. *Carbon N Y.* **82**, 304–313 (2015).
69. Ren, H., Qi, F., Feng, X., Liu, J. & Zhao, Y. Facile synthesis of fluorescent carbon quantum dots with high product yield using a solid-phase strategy. *Molecules* **29**, 1–12 (2024).
70. Papaioannou, N., Titirici, M. M. & Sapelkin, A. Investigating the effect of reaction time on carbon dot formation, structure, and optical properties. *ACS Omega*. **4**, 21658–21665 (2019).
71. Sk, M. A., Ananthanarayanan, A., Huang, L., Lim, K. H. & Chen, P. Revealing the tunable photoluminescence properties of graphene quantum dots. *J. Mater. Chem. C.* **2**, 6954–6960 (2014).
72. Wei, J. & Qiu, J. Unveil the fluorescence of carbon quantum dots. *Adv. Eng. Mater.* **17**, 132–142 (2015).
73. Issa, M. A. et al. Fluorescent recognition of Fe^{3+} in acidic environment by enhanced-quantum yield N-doped carbon dots: optimization of variables using central composite design. *Sci. Rep.* **10**, 1–18 (2020).
74. Barati, A., Shamsipur, M., Arkan, E., Hosseinzadeh, L. & Abdollahi, H. Synthesis of biocompatible and highly photoluminescent nitrogen doped carbon dots from lime: analytical applications and optimization using response surface methodology. *Mater. Sci. Eng. C*. **47**, 325–332 (2015).
75. Costa, J. C. S., Taveira, R. J. S., Lima, C. F. R. A. C., Mendes, A. & Santos, L. M. N. B. F. Optical band gaps of organic semiconductor materials. *Opt. Mater. (Amst).* **58**, 51–60 (2016).
76. Fouad, M. M., Shihata, L. A. & Morgan, E. S. I. An integrated review of factors influencing the performance of photovoltaic panels. *Renew. Sustain. Energy Rev.* **80**, 1499–1511 (2017).
77. Ateia, E. E., Rabie, O. & Mohamed, A. T. Assessment of the correlation between optical properties and CQD preparation approaches. *Eur. Phys. J. Plus*. **139**, 24 (2024).
78. Nugraha, M. W., Sambudi, N. S., Kasmiarno, L. D. & Kamal, N. A. The effect of amino-functionalization on photoluminescence properties of sugarcane bagasse-derived carbon quantum dots. *ASEAN J. Chem. Eng.* **21**, 62–72 (2021).
79. Tuerhong, M., Yang, X. U., & Xue-Bo, Y. I. N. Review on carbon dots and their applications. *Chin. J. Anal. Chem.* **45**, 139–150 (2017).
80. Manjubaashini, N., Bargavi, P. & Balakumar, S. Carbon quantum dots derived from agro waste biomass for pioneering bioanalysis and in vivo bioimaging. *J. Photochem. Photobiol Chem.* **454**, 115702 (2024).
81. Surendran, P. et al. Fluorescent carbon quantum dots from Ananas comosus waste peels: a promising material for NLO behaviour, antibacterial, and antioxidant activities. *Inorg. Chem. Commun.* **124**, 108397 (2021).
82. Ang, W. L. et al. Microwave-assisted conversion of palm kernel shell biomass waste to photoluminescent carbon dots. *Sci. Rep.* **10**, 1–15 (2020).

83. Scimeca, M., Bischetti, S., Lamsira, H. K., Bonfiglio, R. & Bonanno, E. Energy dispersive X-ray (EDX) microanalysis: a powerful tool in biomedical research and diagnosis. *Eur. J. Histochem.* **62**, 89–99 (2018).
84. Ding, H. et al. Surface states of carbon dots and their influences on luminescence. *J. Appl. Phys.* **127**, 231101 (2020).
85. Amloy, S., Lukprang, T., Lertworapreecha, M. & Preechaburana, P. Green synthesis of carbon dots from mangosteen peel for fluorescent cancer cells. *J. Met. Mater. Min.* **34**, 1–8 (2024).
86. Kamal, A. & Hong, S. Carbon quantum dots: synthesis, characteristics, and quenching as biocompatible fluorescent probes. *Biosensor* **15** (99), 1–19 (2025).
87. Sachdev, A., Matai, I. & Gopinath, P. Implications of surface passivation on physicochemical and bioimaging properties of carbon dots. *RSC Adv.* **4**, 20915–20921 (2014).
88. Eskalen, H., Uruş, S., Kavgacı, M., Kalmış, H. V. & Tahta, B. Carbon quantum dots derived from pomegranate peel: highly effective fe(III) sensor. *Biomass Convers. Biorefinery.* **14**, 1201–1214 (2024).
89. Khaledian, S. et al. Rapid detection of diazinon as an organophosphorus poison in real samples using fluorescence carbon dots. *Inorg. Chem. Commun.* **130**, 108676 (2021).
90. Sundaraganesan, N., Ilakiamani, S., Saleem, H. & Mohan, S. FT-Raman, FTIR spectra and normal coordinate analysis of 5-bromo-2-nitropyridine. *Indian J. Pure Appl. Phys.* **42**, 585–590 (2004).
91. Nazar, M., Hasan, M., Wirjosentono, B., Gani, B. A. & Nada, C. E. Microwave synthesis of carbon quantum dots from Arabica coffee ground for fluorescence detection of Fe^{3+}, Pb^{2+}, and Cr^{3+}. *ACS Omega.* **9**, 20571–20581 (2024).
92. Prekodravac, J. et al. Green and facile microwave assisted synthesis of (metal-free) N-doped carbon quantum dots for catalytic applications. *Ceram. Int.* **45**, 17006–17013 (2019).
93. Marković, Z. M. et al. Structural, optical, and bioimaging characterization of carbon quantum dots solvothermally synthesized from o-phenylenediamine. *Beilstein J. Nanotechnol.* **14**, 165–174 (2023).
94. Atchudan, R. et al. Sustainable synthesis of carbon quantum dots from banana peel waste using hydrothermal process for in vivo bioimaging. *Phys. E Low-Dimensional Syst. Nanostruct.* **126**, 114417 (2021).
95. Yang, Z., Liu, C., Gao, Y., Wang, J., & Yang, W. Influence of surface roughness on surface plasmon resonance phenomenon of gold film. *Chin. Opt. Lett.* **14**, 042401–042403 (2015).
96. Eddin, F. B. K. et al. Direct and sensitive detection of dopamine using carbon quantum dots based refractive index surface plasmon resonance sensor. *Nanomaterials* **12**, 1799 (2022).
97. Fauzi, N. I. M., Fen, Y. W., Omar, N. A. S., & Hashim, H. S. Recent advances on detection of insecticides using optical sensors. *Sensors* **21**, 3856 (2021).
98. Nasr, N. et al. A two-fold SPR-SERS sensor utilizing gold nanoparticles and graphene thin membrane as a spacer in a 3D composite structure. *Spectrochim Acta - Part. Mol. Biomol. Spectrosc.* **304**, 123331 (2024).
99. Tseng, W., Bin, Hsieh, M. M., Chen, C. H., Chiu, T. C. & Tseng, W. L. Functionalized gold nanoparticles for sensing of pesticides: a review. *J. Food Drug Anal.* **28**, 521–538 (2020).
100. Mauriz, E. Recent progress in plasmonic biosensing schemes for virus detection. *Sens.* **20**, 4745 (2020).
101. Wu, X. et al. Environmental occurrence, toxicity concerns, and degradation of diazinon using a microbial system. *Front. Microbiol.* **12**, 717286 (2021).
102. Bilal, S., Sami, A. J., Hayat, A., & Ur Rehman, M. F. Assessment of pesticide induced Inhibition of apis mellifera (honeybee) acetylcholinesterase by means of N-doped carbon dots/BSA nanocomposite modified electrochemical biosensor. *Bioelectrochemistry* **144**, 107999 (2022).
103. Baharum, N. A. et al. Highly efficient removal of diazinon pesticide from aqueous solutions by using coconut shell-modified biochar. *Arab. J. Chem.* **13**, 6106–6121 (2020).
104. Hashim, H. S., Fen, Y. W., Omar, N. A. S. & Fauzi, N. I. M. Sensing methods for hazardous phenolic compounds based on graphene and conducting polymers-based materials. *Chemosensors* **9**, 1–40 (2021).
105. Bahamon-Pinzon, D., Moreira, G., Obare, S. & Vanegas, D. Development of a nanocopper-decorated laser-scribed sensor for organophosphorus pesticide monitoring in aqueous samples. *Microchim. Acta.* **189**, 254 (2022).
106. Zhang, C., Qiu, M., Wang, J. & Liu, Y. Recent advances in nanoparticle-based optical sensors for detection of pesticide residues in soil. *Biosensors* **13**, 1–30 (2023).
107. Amirjani, A., Bagheri, M., Heydari, M. & Hesaraki, S. Colorimetric determination of timolol concentration based on localized surface plasmon resonance of silver nanoparticles. *Nanotechnology* **27**, 1811–1820 (2016).
108. Zehani, N., Dzyadevych, S. V. & Kherrat, R. Jaffrezic-Renault, N. J. Sensitive impedimetric biosensor for direct detection of diazinon based on lipases. *Front. Chem.* **2**, 1–7 (2014).
109. Tan, J. et al. Enhanced photoelectric conversion efficiency: a novel h-BN based self-powered photoelectrochemical aptasensor for ultrasensitive detection of diazinon. *Biosens. Bioelectron.* **142**, 111546 (2019).

Acknowledgements

This research was funded by Universiti Putra Malaysia through Putra Grant (GPB/2024/9810900).

Author contributions

Conceptualization, Methodology, Formal analysis, Investigation, Writing – original draft, Writing – review & editing (Nor Afiqah Nor Asri); Conceptualization, Validation, Visualization, Data curation, Writing – review & editing, Resources, Supervision, Project administration, Funding acquisition (Yap Wing Fen); Validation, Visualization, Data curation (Nurul Illya Muhamad Fauzi); Visualization, Resources (Nur Aqilah Kamaruzzaman); Validation, Resources (Rahayu Emilia Mohamed Khaidir and Hazwani Suhaila Hashim); Software (Muhammad Fahmi Anuar and Muhammad Amir Zakwan Mohd Zailani); Visualization (Ahmad Danish Iskandar Mohd Fadzil and Nur Nadia Amira Mahamad Basari); Supervision (Mazliana Ahmad Kamarudin); Methodology and Data curation (Huda Abdullah).

Funding

This research was funded by Universiti Putra Malaysia through Putra Grant (GPB/2024/9810900).

Declarations

Competing interests

The authors declare no competing interests.

Additional information

Correspondence and requests for materials should be addressed to Y.W.F.

Reprints and permissions information is available at www.nature.com/reprints.

Publisher's note Springer Nature remains neutral with regard to jurisdictional claims in published maps and institutional affiliations.